THE ASTROPHYSICAL JOURNAL, 493:680–693, 1998 February 1

INTERPRETING THE HCN/CO INTENSITY RATIO IN THE GALACTIC CENTER

TIMOTHY A. D. PAGLIONE,[1] JAMES M. JACKSON, AND ALBERTO D. BOLATTO[2]
Department of Astronomy, Boston University, 725 Commonwealth Avenue, Boston, MA 02215
AND
MARK H. HEYER
Five College Radio Astronomy Observatory, Lederle Research Tower, University of Massachusetts, Amherst, MA 01003
Received 1997 February 2; accepted 1997 September 8

ABSTRACT

We study the dense molecular gas in the Galactic center using maps of HCN and CO $J = 1 \rightarrow 0$ emission from the central 630 pc of the Milky Way, and images of HCN $J = 3 \rightarrow 2$ emission, which requires high densities for excitation ($n_{H_2} \gtrsim 10^6$ cm^{-3}), from Sgr A and Sgr B. The ratio of integrated HCN and CO $J = 1 \rightarrow 0$ intensities is a sensitive measure of molecular gas pressure, and the ratio of integrated HCN $J = 3 \rightarrow 2$ and $J = 1 \rightarrow 0$ intensities uncovers density enhancements in the maps. However, the HCN/CO ratio is difficult to model without knowing the relative HCN and CO abundances. Furthermore, because of the different filling factors of HCN and CO emission, models that use homogeneous clouds may not be accurate for analyzing the HCN/CO ratio.

Most of the mass traced by HCN and CO in the Galactic center is at high densities ($n_{H_2} \sim 10^4$ cm^{-3}), roughly an order of magnitude higher than cloud densities in the Galactic disk. Most of the dense gas traced by HCN $J = 3 \rightarrow 2$ emission is coincident with star-forming regions and cloud interaction zones, and not necessarily with emission peaks. We smoothed the HCN and CO maps to the typical spatial resolution of extragalactic observations, and repeated the analysis. The single large-scale measurement was sensitive to the mass-weighted average properties of the map. Therefore, if we can extrapolate this result to other spirals, studies such as this are sensitive to the *average* gas properties in galactic nuclei, despite poor spatial resolution.

Subject headings: galaxies: ISM — Galaxy: center — ISM: clouds — ISM: molecules

1. INTRODUCTION

Recent single-dish work has demonstrated the value of HCN as a probe of the dense gas in galactic nuclei (e.g., Solomon, Downes, & Radford 1992; Helfer & Blitz 1993; Jackson et al. 1995; Paglione, Jackson, & Ishizuki 1997a). Because of its high electric dipole moment, HCN requires large gas densities for collisional excitation. Thus, HCN, a relatively abundant interstellar molecule, is an excellent probe of the dense, star-forming gas in galaxies. It is especially luminous in starburst galaxies (Solomon et al. 1992; Helfer & Blitz 1993; Jackson et al. 1996, hereafter Paper 1). Multiline HCN observations have shown that in general, starburst nuclei have both higher average gas densities and larger fractions of dense gas by mass than more quiescent galaxies, such as the Milky Way (Paglione et al. 1997a).

However, the dense gas properties of normal spiral galactic nuclei are only just now being studied. The ratio of integrated HCN and CO $J = 1 \rightarrow 0$ intensities (defined here as $\mathscr{R}$) has been the most widely used density probe, since these lines are easy to observe and can be detected in many galaxies (Helfer & Blitz 1993; Aalto et al. 1995; Paper 1). A high HCN/CO ratio indicates a large molecular gas density because the critical density required to collisionally excite HCN is higher than that required to excite CO. Unfortunately, because the HCN/CO ratio may be a strong function of the spatial scale of the observations, the results are difficult to compare from galaxy to galaxy. Also, modeling $\mathscr{R}$ is problematic because of the unknown abundances of HCN and CO in any source.

The goals of this paper are to address these two problems by (1) studying the dense gas in the center of a normal galaxy at high sensitivity and spatial resolution, (2) determining the utility of the HCN/CO ratio as a probe of the gas properties in galaxies, and (3) quantifying the effects of the usual modeling assumptions on the inferred cloud properties. We completed a survey of the HCN and CO $J = 1 \rightarrow 0$ emission from the central 630 pc of the Milky Way at 50″ (2 pc) sampling (Paper 1). The Milky Way is a good choice for a reference quiescent galaxy because it is observable at the highest spatial resolution and sensitivity of any galaxy. Also, the star formation rate and FIR luminosity are much lower in the Galactic center than in starburst nuclei (Solomon et al. 1992; Morris 1993). However, to compare Galactic and extragalactic data on the same spatial scales, the Milky Way must be studied over a large angular area. To this end, we utilized innovative techniques and instruments to map large regions of the sky toward the Galactic center.

We use the ratio of integrated HCN and CO $J = 1 \rightarrow 0$ intensities, $\mathscr{R}$, and, for comparison, the ratio of integrated HCN $J = 3 \rightarrow 2$ and $J = 1 \rightarrow 0$ intensities to estimate the gas properties of the clouds in the central 630 pc of the Galaxy. Although the HCN $J = 3 \rightarrow 2$ line is more difficult to observe, the HCN $J = 3 \rightarrow 2/J = 1 \rightarrow 0$ ratio is easier to analyze because the problem of unknown relative abundances is eliminated.

2. OBSERVATIONS

The HCN and CO $J = 1 \rightarrow 0$ maps of the Galactic center used here were observed between 1993 and 1994 with the 15

[1] Current address: Instituto Nacional de Astrofísica, Óptica y Electrónica, Apartado Postal 216 y 51, 72000 Puebla, Pue, México; paglione@inaoep.mx.
[2] Also Departamento de Astronomía, Universidad de la República, Montevideo, Uruguay.

beam focal plane array QUARRY (Erickson et al. 1992) at the 14 m Five College Radio Astronomy Observatory (FCRAO) in New Salem, MA. We mapped within the ranges of Galactic longitude and latitude $-2\overset{\circ}{.}13 \leq l \leq 2\overset{\circ}{.}13$ and $-0\overset{\circ}{.}3 \leq b \leq 0\overset{\circ}{.}2$, corresponding to 630 pc × 75 pc at the distance of the Galactic center ($D = 8.5$ kpc). The pixels are spaced every 50″ (2 pc linear scale). Further details of the observations are given in Paper 1.

We observed the HCN $J = 3 \rightarrow 2$ emission ($v_0 = 265.886$ GHz) from the Galactic center remotely with the National Radio Astronomy Observatory (NRAO)[3] 12 m at Kitt Peak, Arizona in 1995 April. We used the facility 260–300 GHz receiver, with typical system temperatures of 1300–1600 K. We used the facility filterbank spectrometers, consisting of 256 channels of 2 MHz width. The main beam efficiency and FWHM were 0.5 and 24″, respectively. Calibration was done using the chopper wheel method, and with observations of W49 and Sgr B2 in position-switching mode.

For fast mapping, we used the "on the fly" (OTF) technique (J. Mangum 1995, private communication) to make R.A. × decl. = 10′ × 10′.5 maps centered on the Sgr A and Sgr B molecular clouds (R.A. = $17^h42^m28^s$, decl. = −29°01′30″ and R.A. $17^h44^m11^s$, decl. = −28°22′30″, respectively). The maps were created by scanning 10′ in right ascension at a rate of 10″ s^{-1}. The observations are sampled every 0.1 s as the dish continues to scan. The position of the dish is monitored every 0.01 s to ensure accurate placement of observed data points in the final map. The 90 rows in each map are separated by 7″ to achieve an oversampling in declination of roughly a factor of 3.

The OTFUV and SDGRD routines of the NRAO AIPS reduction package were used to grid the data into cubes of 43 × 45 map positions and 256 velocity channels. The map pixels are separated by 14″. A parabolic baseline was removed from each gridded spectrum.

3. PHYSICAL PROPERTIES OF THE DENSE GAS IN THE GALACTIC CENTER

3.1. *The* HCN/CO *Ratio*

To determine the physical conditions of the emitting gas in the Galactic center, we performed single-component model calculations of non-LTE HCN and CO excitation, assuming that the emission originates in unresolved, homogeneous, spherical clouds. A photon escape probability function was included to account for the radiative excitation of optically thick lines (see Stutzki & Winnewisser 1985 and references therein).

The emission from the first eight levels of HCN and the first 11 levels of CO were modeled. We used the CO collision rates of Flower & Launay (1985) and the HCN collision rates of Green & Thaddeus (1974). The HCN/CO intensity ratio was modeled by assuming three different values for the relative abundances of HCN and CO: [HCN]/[CO] = 10^{-4}, 2.5×10^{-4}, and 10^{-3}, where [Y] is defined as the abundance of molecule Y with respect to molecular hydrogen. These ratios cover the range of predicted and observed values for dense clouds (e.g., Blake et al. 1987; Bergin, Langer, & Goldsmith 1995).

[3] The National Radio Astronomy Observatory is a facility of the National Science Foundation operated under cooperative agreement by Associated Universities, Inc.

3.1.1. *Modeling Procedure*

It is difficult with only two lines to restrict the range of parameter space to be explored. Our goal here is to understand how the usual assumptions for doing so influence the inferred gas properties. Therefore, the temperature and column density are constrained in the typical way, by assuming that they are directly proportional to the CO intensity. The density is determined from $\mathscr{R}$. The only free parameters are the beam-filling factor and the abundances of HCN and CO. The homogeneous cloud model also implies that the beam-filling factors of HCN and CO are equal (clearly a poor assumption, but adding more free parameters is unwarranted with only two lines). The impact of these assumptions are analyzed in later sections.

The CO column density per velocity interval, $N_{CO}/\Delta v$, was estimated from the CO intensity by assuming

$$\frac{N_{CO}}{\Delta v} = \frac{I_{CO} X_{CO}[CO]}{\phi \, \Delta v} , \tag{1}$$

where ϕ is the area beam-filling factor and X_{CO} is the conversion factor of CO integrated intensity to H_2 column density. Although the standard value for X_{CO} is $\sim 3 \times 10^{20}$ cm^{-2}/(K km s^{-1}), this was derived from cold disk clouds (e.g., Scoville et al. 1987). We use instead the smaller value of $X_{CO} = 5 \times 10^{19}$ cm^{-2}/(K km s^{-1}), valid for the metal-rich, turbulent clouds of the inner Galaxy (Sodroski et al. 1995 and references therein). We use [CO] = 8×10^{-5} (Frerking, Langer, & Wilson 1982). The FWHM velocity width Δv is calculated at each position from the second moment of the CO spectrum,

$$\sigma_v = \left[\frac{\int T(v - \langle v \rangle)^2 \, dv}{\int T \, dv} \right]^{1/2} \tag{2}$$

and

$$\Delta v = 2\sqrt{\ln 4}\sigma_v . \tag{3}$$

Equation (3) corrects the velocity dispersion so that for a Gaussian line shape, Δv equals the FWHM of the spectrum. Nearly all of the dominant emission peaks have roughly Gaussian profiles at our velocity resolution of 17 km s^{-1}.

The kinetic temperature T_k at each position in the HCN/CO ratio map can be estimated from T_{CO}, the peak observed brightness temperature of CO, since

$$T_{CO} = \phi(T_{ex} - T_{bg})(1 - e^{-\tau}) , \tag{4}$$

where T_{ex} is the excitation temperature, T_{bg} is the 2.7 K background temperature, and τ is the CO optical depth. (All observed temperatures have been adjusted to the main beam scale.) In general, $T_{ex} \leq T_k$ and

$$T_k \geq \frac{T_{CO}}{\phi(1 - e^{-\tau})} + T_{bg} \tag{5}$$

or

$$T_k = \frac{T_{CO}}{f} + T_{bg} , \tag{6}$$

where we define f as

$$0 < f \leq \phi(1 - e^{-\tau}) \leq 1 . \tag{7}$$

Note that $f \approx \phi$, since CO is typically thermalized and optically thick ($T_{ex} \approx T_k$ and $\tau \gg 1$). However, the kinetic temperature and beam-filling factor are not directly calculable

in this analysis. T_k is estimated by choosing f_1 (an initial value for f), and setting $\phi = f_1$. The model then predicts a CO intensity and optical depth. By comparing model and observed CO intensities, the beam-filling factor is estimated from

$$\phi = \frac{T_{\rm CO}(\text{observed})}{T_{\rm CO}(\text{predicted})} . \quad (8)$$

If equation (7) is not satisfied, f (and therefore T_k) is adjusted to lower or raise the predicted $T_{\rm CO}$ accordingly (eq. [6]), and the process is repeated. The procedure stops when the variations in T_k fall below 5% and equation (7) holds. Convergence is typically reached in less than a few iterations.

3.1.2. *Effects of Assumptions and Model*

In this section, we discuss how the model assumptions could affect the inferred gas properties. This discussion is important since often extragalactic analyses are also poorly constrained due to a lack of data. (They also suffer from poor spatial resolution and sensitivity, which we address later.)

The inequality in equation (7) implies that ϕ may be poorly estimated. For high values of f_1, requiring that $\phi \geq f_1$ eliminates any low beam-filling factor solutions, thus underestimating T_k and $N_{\rm CO}/\Delta v$. Conversely, for low values of f_1, equation (7) can be satisfied with very small beam-filling factors. Although HCN/CO does not vary much with T_k, at high column densities (where trapping is important), the inferred densities may be poorly determined. The relation between density and ϕ is tested in the following section.

It is also difficult to separate beam-filling and optical depth in equation (7). However, $\tau > 1$ almost always, so this problem should be minor.

Because the critical density of HCN is a factor of ~ 300 higher than that of CO, the emission from both molecules will not come from the same regions. This was shown by modeling the emission from CO and another high dipole moment molecule, CS (Gierens, Stutzki, & Winnewisser 1992). Therefore, the observed HCN/CO ratio (and thus the density) is a lower limit to the actual value in the dense, HCN-emitting regions of interest, and a homogeneous cloud may be a poor model. However, as mentioned before, this problem is very difficult to constrain with only two lines, so it is set aside for future work.

3.1.3. *Model Results*

The results of one model are shown in Figure 1 for 7155 positions in the HCN and CO images of Paper 1. Here, the fraction of the total mass (estimated from $M_{\rm H_2} \propto I_{\rm CO}$, the observed CO intensity) is displayed as a function of the model variables, assuming [HCN]/[CO] $= 2.5 \times 10^{-4}$ and $f_1 = 0.1$. The mass-weighted average values of the parameters in Figure 1 are given in Table 1.

A wide range of temperatures and CO column densities are found for the clouds within the central 630 pc of the Milky Way. These solutions are simply scaled by the beam-filling factor that is constrained by the choice of f_1.

The distribution of mass as a function of T_k is truncated at low temperatures because map positions without significant emission have been discarded from the analysis. Thus, "cold" regions, which are also confused within the noise level of our map, have been ignored. We find $\langle T_k \rangle \approx 75$ K, with roughly 75% of the mass at temperatures below 100 K. This result matches that found from NH_3 measurements of the same clouds (Hüttemeister et al. 1993). Therefore, this model solution is used in subsequent analysis and discussion.

The distribution of mass with density in Figure 1 is dominated by a narrow peak near $n_{\rm H_2} = 10^4$ cm^{-3}. To estimate the dependence of the mean density on the input parameters, $\langle n \rangle$ is plotted as a function of f_1, $\langle \phi \rangle$, and [HCN]/[CO] in Figure 2. The mean density is directly proportional

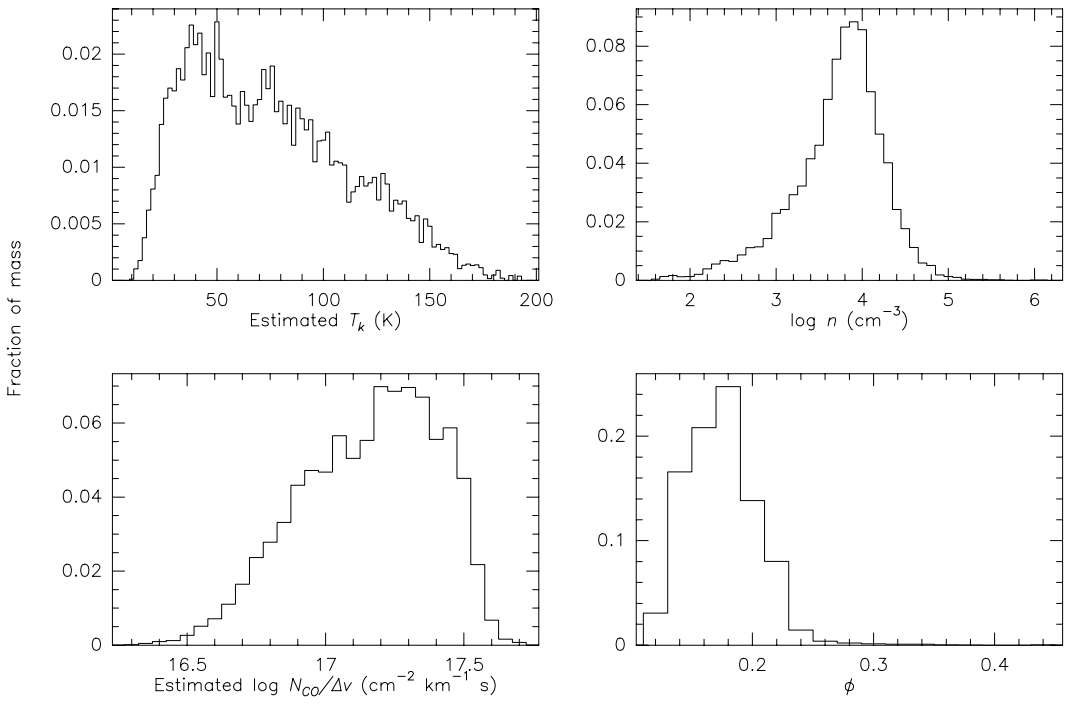

FIG. 1.—Fraction of mass (estimated from $M \propto I_{\rm CO}$) at a particular kinetic temperature (*upper left panel*), CO column density per velocity interval (*lower left panel*), H_2 density (*upper right panel*), and beam-filling factor (*lower right panel*. Here $f_1 = 0.1$ and [HCN]/[CO] $= 2.5 \times 10^{-4}$.

TABLE 1

MODEL RESULTS: MEAN VALUES AND 1 σ DISPERSIONS

f_1	[HCN]/[CO]	$\langle T_k \rangle$ (K)	$\langle \log (N_{HCN}/\Delta v) \rangle$ (cm^{-2} km^{-1} s)	$\langle \log n \rangle$ (cm^{-3})	$\langle \phi \rangle$
1.0.....	2.5×10^{-4}	11 ± 5	16.3 ± 0.2	4.4 ± 0.4	0.97 ± 0.03
0.5.....	1.0×10^{-4}	16 ± 8	16.5 ± 0.3	4.7 ± 0.4	0.65 ± 0.04
0.5.....	2.5×10^{-4}	16 ± 8	16.5 ± 0.3	4.2 ± 0.4	0.65 ± 0.04
0.5.....	1.0×10^{-3}	17 ± 8	16.5 ± 0.3	3.4 ± 0.4	0.72 ± 0.07
0.2.....	2.5×10^{-4}	38 ± 19	16.9 ± 0.3	3.9 ± 0.5	0.30 ± 0.04
0.1.....	2.5×10^{-4}	75 ± 37	17.2 ± 0.2	3.7 ± 0.5	0.17 ± 0.03

to $\langle \phi \rangle$, the average beam-filling factor. This dependence comes about because $N_{CO}/\Delta v$ is inversely proportional to ϕ, and at low column densities (optical depths), trapping is minor, so a higher density is needed to produce a given HCN/CO ratio. However, the mean density is more sensitive to the assumed HCN abundance. A higher abundance increases the column density of HCN, thus decreasing, because of radiative trapping, the density needed to generate a particular HCN/CO ratio.

3.1.4. *Model Biases*

To ensure that the above solutions were not the result of biases in the method or model, the same procedure was done for a set of 1000 HCN and CO intensities, generated from a set of random values of n_{H_2}, $N_{CO}/\Delta v$, ϕ, and T_k. The only constraint on the inputs was that the resulting CO intensities had to be above the clip level used in the Galactic center HCN/CO map. Three simulations were run to solve for these gas properties, given the fabricated HCN and CO intensities. Biases exist if the original distributions of n_{H_2}, $N_{CO}/\Delta v$, ϕ, and T_k are not recovered. [HCN]/[CO] was fixed at 2.5×10^{-4}.

Histograms of the input distributions are displayed in Figure 3. Shown are the average values of the mass fraction from three simulations, and the 1 σ dispersions. The distribution of mass with density is flat, while the other variables are affected by the lower limit set on the CO intensity. Not surprisingly, most of the mass (intensity) is in optically thick (high column density), hot gas with high beam-filling factors.

Figure 4 shows the model solutions for n_{H_2}, $N_{CO}/\Delta v$, ϕ, and T_k based on the fabricated HCN and CO intensities (for $f_1 = 0.1$ and [HCN]/[CO] $= 2.5 \times 10^{-4}$). Figure 5 compares the output solutions with the inputs. Because ϕ is not solved for exactly, the kinetic temperature, column density, and beam-filling factor show bias. The model indicates more mass at low T_k, $N_{CO}/\Delta v$, and ϕ. The mass distribution with column density also narrows.

In contrast, the output and input densities agree well except at very high and very low densities. Above 10^6 cm^{-3}, the HCN/CO ratio drops with density as HCN becomes thermalized, and there is no unique solution for density (the model chooses the lower value). Also, if the observed $\mathscr{R}$ is greater than the model at all densities, the point with the highest HCN/CO ratio is taken. This density is near 10^6 cm^{-3}, and explains the extra mass near this value. Below 10^2 cm^{-3}, both CO and HCN are subthermally excited and the HCN/CO ratio is not as sensitive to changes in density. Therefore, the model reproduces the input densities well for $10^2 < n_{H_2} < 10^6$ cm^{-3}, and the density distribution in Figure 1, which shows over 30% of the total mass at a density of $\sim 10^4$ cm^{-3}, is probably not an artifact of the molecular probes, model, or analysis procedure.

HCN and CO intensities were also generated using the Galactic center solutions as inputs. Unlike the cases with randomly generated parameters, there is extremely good agreement between input and output in this exercise. Apparently, more self-consistent or realistic cloud properties are well reproduced by the model. Despite the expected biases, none of the distributions are greatly affected (see Fig. 6). With each iteration, the peaks all increase slightly and the dispersions decrease. The deviations in the means are well within 1 σ.

3.1.5. *The Dependence of* HCN/CO *on Gas Properties*

Figure 7 shows the HCN/CO ratio versus the estimated physical properties of the gas at each of the 7155 modeled positions in our Galactic center map. There is no clear

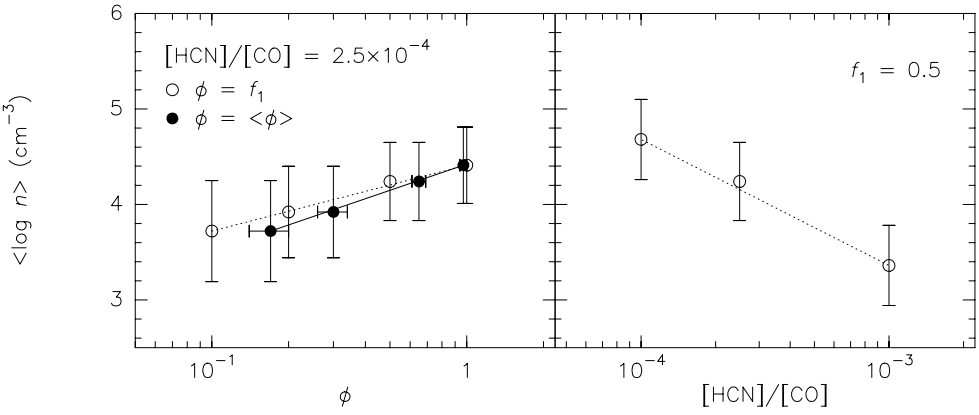

FIG. 2.—*Left panel*: Dependence of the mass-weighted mean density on the mean beam-filling factor (*dots and solid line*) and f_1 (*open circles and dotted line*) for [HCN]/[CO] $= 2.5 \times 10^{-4}$. *Right panel*: Dependence of $\langle \log n \rangle$ on the abundance ratio [HCN]/[CO] for $f_1 = 0.5$.

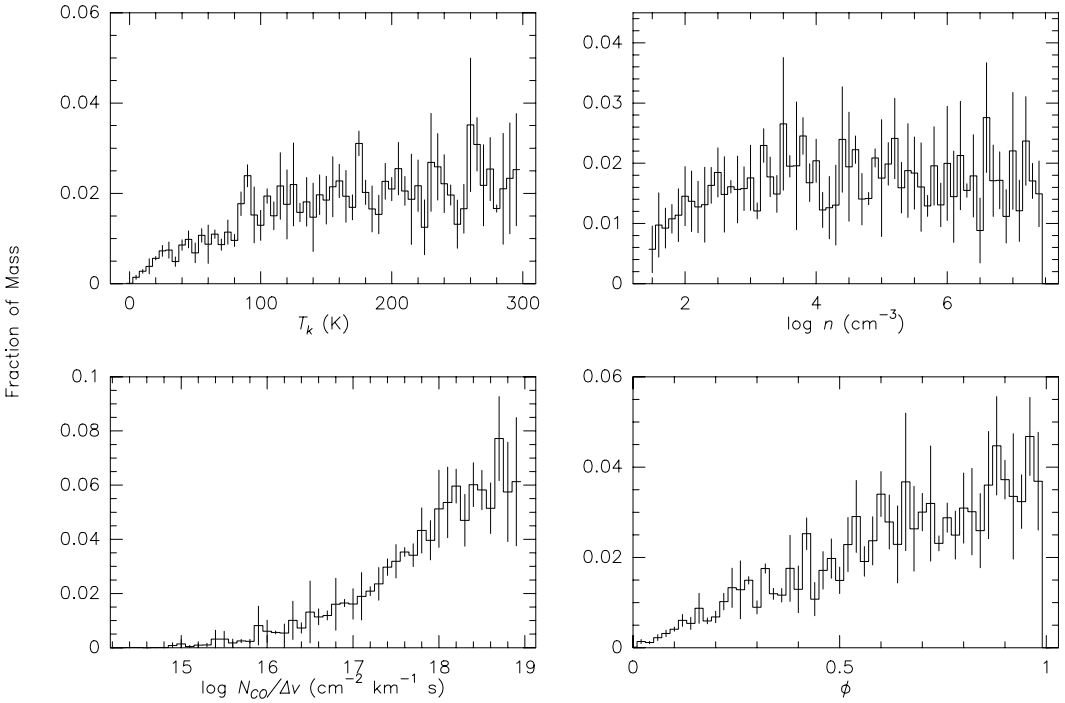

FIG. 3.—Random input parameters displayed as in Fig. 1. Histograms are the average of three sets of random T_k, $N_{CO}/\Delta v$, n_{H_2}, and ϕ inputs; error bars show the dispersion.

correlation between ϕ and the HCN/CO ratio. However, $\mathscr{R}$ rises with kinetic temperature, and it is tightly correlated with density and pressure, $P = nT_k$. Therefore, according to our model, the HCN/CO ratio may be a sensitive measure of molecular gas pressure over orders of magnitude in $\mathscr{R}$ and P. Recall, however, that the derived gas density depends strongly on the assumed [HCN]/[CO] abundance ratio and on ϕ.

The tightness of the correlation between thermal gas pressure and $\mathscr{R}$ is curious. It was expected that $\mathscr{R} \propto n_{H_2}$, but the model indicates that $\mathscr{R}$ is fairly insensitive to or drops with T_k (except for very high values of $\mathscr{R}$, T_k, and n_{H_2}).

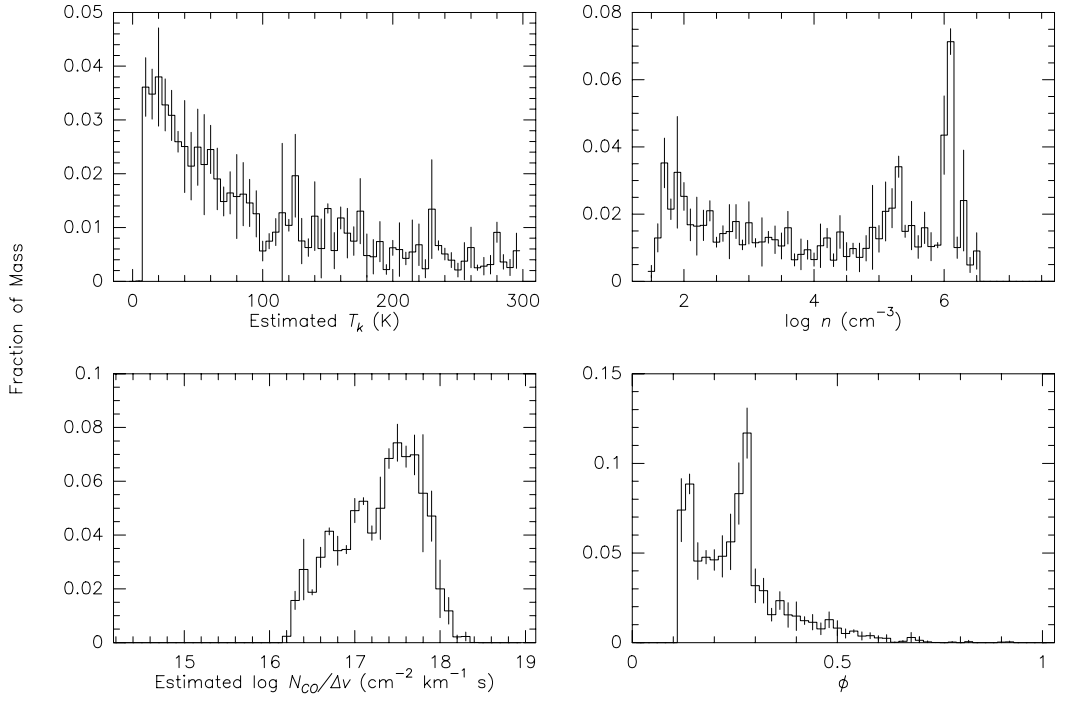

FIG. 4.—Output of model using the random inputs of Fig. 3. Here $f_1 = 0.1$ and [HCN]/[CO] = 2.5×10^{-4}

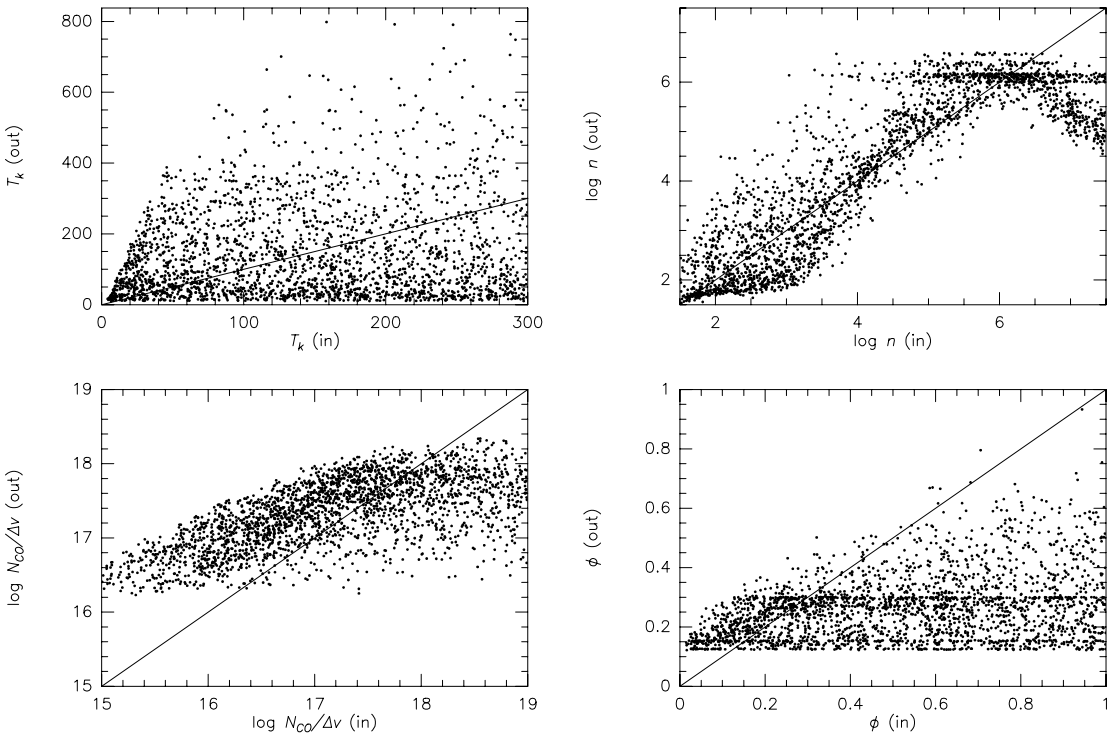

FIG. 5.—Model solutions plotted against random inputs. A slope of unity is indicated.

However, Figure 7 shows $\mathscr{R}$ rising with T_k. Also, a tight correlation results if the dispersion in column densities is very small, as is the case here. These points raise questions as to whether T_k and $N_{CO}/\Delta v$ are estimated properly.

The small dispersion in column densities (Figs. 1, 4, and 5) may result from using a constant CO to H_2 conversion factor in spite of the fact that it is predicted to change with cloud conditions (e.g., Sakamoto 1996). In fact, the dispersion in column density found from modeling $H^{13}CN$ and NH_3 emission from these clouds is 2–4 times that derived from a simple conversion of CO intensity (Paglione et al. 1997b; Hüttemeister et al. 1993). In addition, the CO abun-

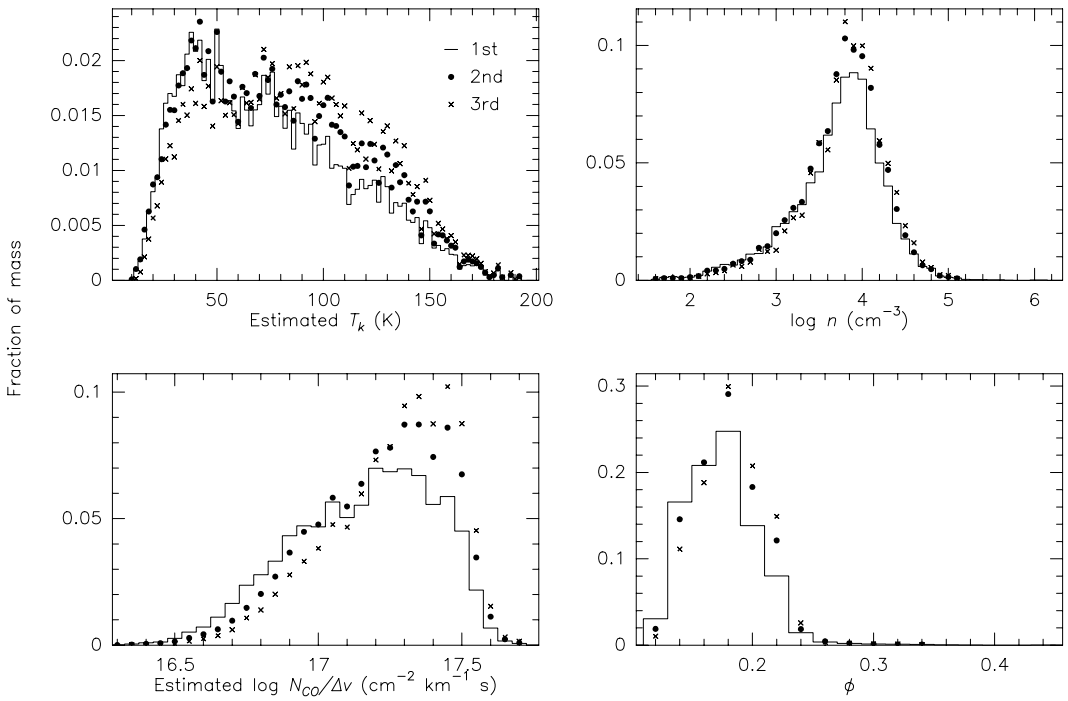

FIG. 6.—Solutions for the mass distributions in the Galactic center after one (*histogram*), two (*dots*), and three (*crosses*) iterations of the model. Here $f_1 = 0.1$ and [HCN]/[CO] = 2.5×10^{-4}.

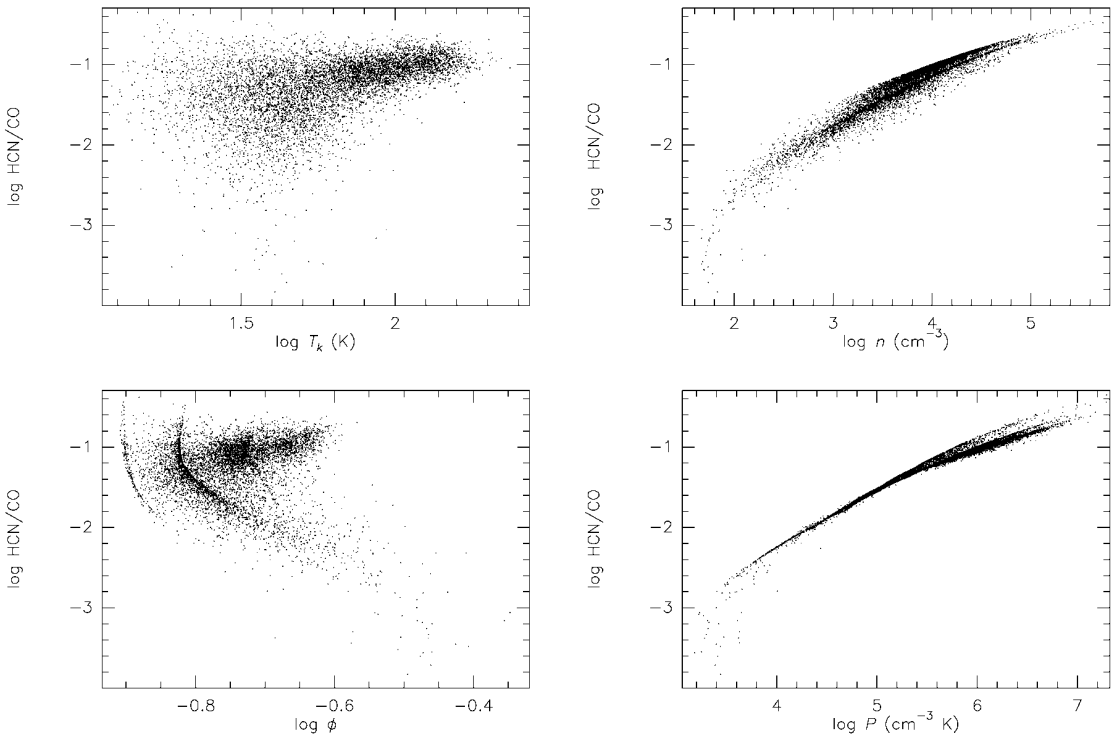

FIG. 7.—The HCN/CO ratio versus T_k (*upper left panel*), ϕ (*lower left panel*), n_{H_2} (*upper right panel*), and pressure $P = nT_k$ (*lower right panel*), for each modeled position in the Galactic center. Here $f_1 = 0.1$ and [HCN]/[CO] = 2.5×10^{-4}.

dance changes markedly from cloud core to surface (Blake et al. 1987). Therefore, a tight correlation may result because a constant CO to H_2 conversion does not properly uncover the structure in these dense clouds.

That the HCN/CO ratio increases with T_k when the model shows no such trend is more difficult to understand. This effect probably arises from estimating T_k from T_{CO} (eq. [7]), and from the physics ignored in the homogeneous cloud model. The worst assumption of the model is that ϕ(HCN) = ϕ(CO). We define ϕ as $\mathcal{N}A_c/A_B$, where $\mathcal{N}$ is the number of clumps in the beam, and A_c and A_B are the clump and beam radii, respectively. It can be shown that A_c(HCN) increases with T_k. According to the model, T_{HCN} rises roughly as $(n_{H_2})^{1/2}$. The density of a typical clump follows a power law with radius $n_{H_2} \propto r^{-3/2}$ (Gierens et al. 1992 and references therein). Therefore, T_{HCN} should decrease with radius as $r^{-3/4}$. In comparison, T_{CO} is fairly insensitive to n_{H_2}, so it does not change with r until the clump edge is reached. This radial structure was found by Gierens et al. (1992) by modeling the molecular emission from a clump. Therefore, as T_{CO} and T_{HCN} increase with T_k, A_c(HCN) increases, but A_c(CO) does not.

The number of HCN-emitting clumps $\mathcal{N}$ will also increase with T_k. Within the beam are clumps of various densities, some of which are dense enough to have detectable HCN emission. CO emission is presumably seen from every clump. As T_k increases, HCN emission will be detectable from less-dense clumps, thus increasing $\mathcal{N}$(HCN) while $\mathcal{N}$(CO) remains unchanged.

This argument can be tested by estimating T_k by other means. In accordance with the model, no correlation between T_k and $\mathcal{R}$ is found when T_k is derived from $H^{13}CN$ or NH_3 measurements (Paglione et al. 1997b; Hüttemeister et al. 1993). Therefore, although the HCN/CO ratio may be a good measure of gas pressure, the real scatter is most likely higher than shown in Figure 7.

3.2. *Comparison with Other Galaxies: Modeling the Large-Scale Emission*

To compare the HCN and CO spectra from the Milky Way to those from other galaxies, the QUARRY maps were convolved to one "beam" with a FWHM of 630 pc, centered on $l = 0°$, $b = 0°$. This linear scale corresponds to 26″ at a distance of 5 Mpc, comparable to observations of nearby galaxies with the IRAM 30 m (Rieu et al. 1992; Aalto et al. 1995). The maps can also be compared to interferometric data (Paglione, Tosaki, & Jackson 1995), although to date few galaxies have been studied in HCN (Helfer & Blitz 1997; Kohno et al. 1996; Brouillet & Schilke 1993; Jackson et al. 1993b; Downes et al. 1992). The convolved HCN and CO spectra (Fig. 8) have integrated intensities (I_{HCN} = 9.8 K km s^{-1} and I_{CO} = 113.3 K km s^{-1}) and peak main-beam brightness temperatures (T_{HCN} = 67 mK and T_{CO} = 534 mK) typical of nearby quiescent galaxies (Helfer & Blitz 1993; Aalto et al. 1995). In fact, after lowering the signal-to-noise ratio of the Milky Way spectra, they are qualitatively indistinguishable from extragalactic observations.

The convolved data can be used solve for the physical conditions of the molecular gas in the Galactic center over large scales with techniques from § 3.1. The HCN/CO ratio may be underestimated, because more CO than HCN emission is likely to lie outside of our rectangular map (Paper 1; Paglione 1996). However, we overlook this correction since it represents less than a 10% change in $\mathcal{R}$, within the observational uncertainties.

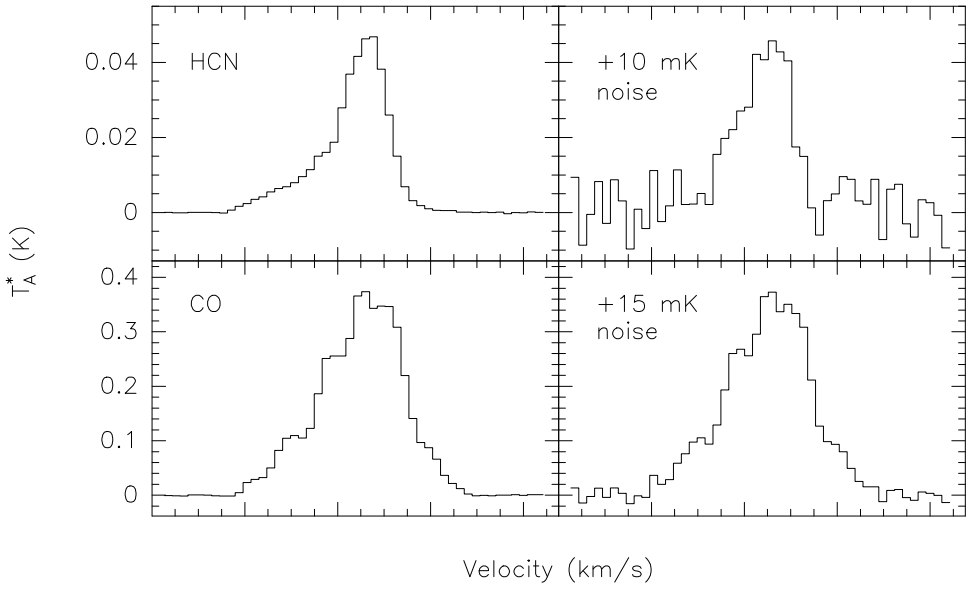

FIG. 8.—Spectra of the HCN (*top left panel*) and CO (*bottom left panel*) emission from the Milky Way convolved to 630 pc resolution. The right frames are the corresponding spectra with noise added to simulate the signal-to-noise ratio of typical extragalactic data.

Initially, ϕ is constrained from a simple geometric scaling of the map solution $\langle\phi\rangle$, using the ratio of the area of the rectangular map to that of the circular Gaussian beam,

$$\phi \lesssim \langle\phi\rangle \frac{\Delta l\, \Delta b}{\pi(\mathrm{FWHM}/2)^2(\ln 2)^{-1}}\,. \tag{9}$$

With $\Delta l = 630$ pc, $\Delta b = 75$ pc, and FWHM = 630 pc, we find $\phi \sim 0.02$. Therefore, $T_k > 30$ K and log $N(\mathrm{CO})/\Delta v \sim 17.1$ cm^{-2} km^{-1} s. With these constraints, and given $\mathscr{R} = 0.08 \pm 0.02$ and [HCN]/[CO] $= 2.5 \times 10^{-4}$, then log $(n/\mathrm{cm}^{-3}) \sim 3.8 \pm 0.4$. These solutions, within the uncertainties, are identical to the mass-weighted mean values found by modeling each position in the original QUARRY map (Table 1, Fig. 1). Therefore, this technique is sensitive to the *average* properties of the molecular gas in the central 630 pc of the Milky Way. If these results may be generalized, then *analyses of the large-scale molecular emission in galactic nuclei probe the mean properties of their cloud populations.* Note that this comparison may only be valid in the HCN-emitting regions of galaxies.

3.3. *Cloud Stability*

With their densities estimated, we can now assess the stability of the dense clouds in the Galactic center against tidal disruption. In Figure 9, the mean density and density dispersion as functions of the projected distance r from Sgr A* are compared to the critical density required for tidal stability. This critical density was based on a power-law mass distribution in the central Galaxy proportional to $r^{1.2}$, containing a central point mass of $3.6 \times 10^6\ M_\odot$ (Sanders & Lowinger 1972). The cloud density required to withstand the tidal forces of the Galactic center is proportional to $r^{-1.8}$ (Güsten & Downes 1980; Ho et al. 1985). Figure 9 shows that within $\sim$100 pc (projected distance) of the Galactic center, much of the mass traced by HCN and CO $J = 1 \rightarrow 0$ emission at our resolution is not dense enough to be self-gravitating. Thus, star formation in this region is suppressed (cf. Morris 1993) and must be a result of other processes, such as cloud collision and shock compression. In support of this scenario, the star-forming regions in the Sgr A clouds do in fact seem to be affected by local shocks (Ho et al. 1985; Serabyn, Lacy, & Achtermann 1992). They may also be bound by external pressure (Spergel & Blitz 1992). In contrast, much of the gas at $\sim$80 and 250 pc, which corresponds to major cloud features and massive star-forming regions such as Sgr B, Sgr C, and the $l = 1.^\circ5$ complex, is stable against tidal disruption.

This analysis is hampered by the fact that the distances of these clouds from Sgr A* are not well known. However, much evidence indicates that at least the Sgr A clouds reside near the Galactic center (e.g., Güsten & Downes 1980). Therefore, the cloud features in Sgr A traced by CO and HCN are unstable to tidal disruption and must be bound by external pressure or other influences.

3.4. *HCN $J = 3 \rightarrow 2$ Emission from the Milky Way*

In the previous analysis, the ratio of the abundances of HCN and CO at each position was a free parameter, and

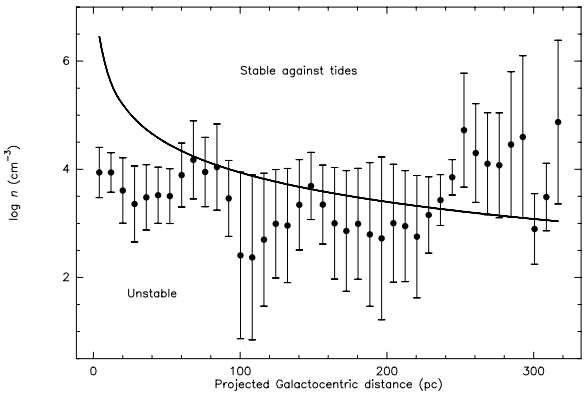

FIG. 9.—Mean density and density dispersion as functions of projected distance from Sgr A*. The data are binned roughly every 8 pc. Curve shows the density required for stability against tidal forces (Ho et al. 1985).

assumed to be constant with position. However, this ratio is known to vary by factors of several within star-forming clouds (e.g., Blake et al. 1987) and is not well known across the Galactic center. Our analysis has also shown that the abundances have a profound effect on the inferred gas density (Fig. 2). Therefore, this variable must be either constrained or eliminated. The HCN/CO ratio is also difficult to model because of the different beam-filling factors of CO and HCN, and because there may not be a unique density solution (Figs. 5 and 10).

Therefore, although the HCN/CO ratio is easier to observe in many sources, and § 3.1 illustrates its usefulness, $\mathscr{R}$ may not be the best tracer of high-density gas in galaxies. The HCN $J = 3 \rightarrow 2/J = 1 \rightarrow 0$ intensity ratio is preferable, in order to eliminate the problem of unknown relative abundances. Figure 10 shows $\mathscr{R}$ and HCN $J = 3 \rightarrow 2/J = 1 \rightarrow 0$ as functions of n_{H_2} for two values of column density. Owing to the high critical density of the HCN $J = 3 \rightarrow 2$ line, HCN $J = 3 \rightarrow 2/J = 1 \rightarrow 0$ rises with density over a very large range, unlike $\mathscr{R}$, which peaks near the critical density of the HCN $J = 1 \rightarrow 0$ line of $\sim 10^6$ cm^{-3}. Another advantage is that the HCN $J = 1 \rightarrow 0$ and $J = 3 \rightarrow 2$ emission arise in nearly the same regions, since their critical densities are more similar. In contrast, the critical density of the HCN $J = 1 \rightarrow 0$ line is over 300 times higher than that of CO $J = 1 \rightarrow 0$. Therefore, although their beam-filling factors are most likely not equal, HCN $J = 3 \rightarrow 2/J = 1 \rightarrow 0$ is more appropriate than $\mathscr{R}$ in the context of the homogeneous cloud model. HCN $J = 3 \rightarrow 2$ emission has also been proven to be a useful probe of dense gas in galaxies (Paglione et al. 1997a). Thus, using HCN $J = 3 \rightarrow 2/J = 1 \rightarrow 0$ to estimate the densities of molecular clouds in the Galactic center employs the same techniques as are used to study external galaxies.

3.4.1. *Results*

Because of the high opacity of the atmosphere at 265 GHz, mapping was limited to the two regions with the highest HCN luminosities, the giant molecular cloud complexes Sgr A and Sgr B. Integrated intensity maps of the HCN $J = 3 \rightarrow 2$ emission from these clouds are shown in Figures 11 and 12. Many of the features in these maps are seen in the $J = 1 \rightarrow 0$ data as well (Paper 1). Three peaks are seen in HCN $J = 3 \rightarrow 2$ integrated intensity toward Sgr A, corresponding to (in order of increasing longitude) the "20 km s^{-1}" cloud, the circumnuclear ring (CNR), and the "50 km s^{-1}" cloud (Güsten 1989; Jackson et al. 1993a). Bright emission is seen at the position of the Sgr B2 main continuum source (Benson & Johnston 1984), and the peak near the edge of the map ($l = 0.^\circ77$, $b = -0.^\circ06$) is nearly coincident with FIR source 38 from the survey of Odenwald & Fazio (1984). The emission below Sgr B2 near $b = -0.^\circ1$ has no obvious counterpart in the infrared or radio. Both of these peaks are seen in $H^{13}CN$ $J = 1 \rightarrow 0$ emission (Paglione et al. 1997b).

3.4.2. *Modeling*

The HCN $J = 3 \rightarrow 2$ data were convolved to the 58″ beam size and 17 km s^{-1} velocity resolution of the $J = 1 \rightarrow 0$ observations, and regridded to match the QUARRY map. The HCN $J = 3 \rightarrow 2/J = 1 \rightarrow 0$ ratio is calculated from the ratio of the main beam integrated intensities at each position in the HCN $J = 1 \rightarrow 0$ map. This ratio was modeled just as in § 3.1. The kinetic temperature and column density are initially constrained by the CO intensity at each position, but Δv is determined from the second moment of the HCN $J = 3 \rightarrow 2$ spectra, ϕ is estimated from the HCN $J = 1 \rightarrow 0$ brightness temperature and optical depth, and n_{H_2} is estimated from HCN $J = 3 \rightarrow 2/J = 1 \rightarrow 0$.

3.4.3. *Model Results*

The model results for Sgr A and Sgr B are listed in Table 2 and shown in Figures 13 and 14 (for $f_1 = 0.1$). The distributions of T_k and HCN column density per velocity interval for the two complexes are quite different. The gas in Sgr

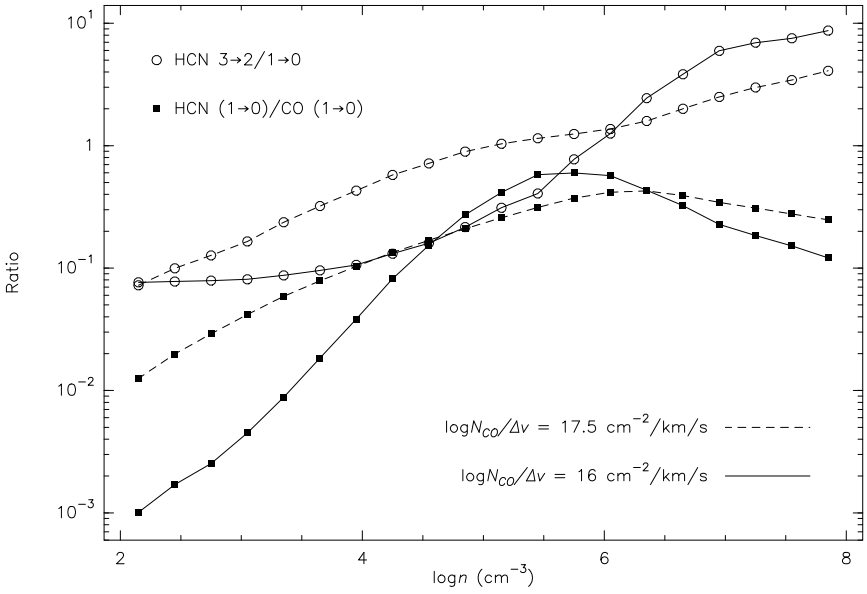

FIG. 10.—HCN $J = 3 \rightarrow 2/J = 1 \rightarrow 0$ (*circles*) and $\mathscr{R}$ (*squares*) as functions of density for log $N_{CO}/\Delta v = 16$ cm^{-2} km^{-1} s (*solid lines*) and 17.5 cm^{-2} km^{-1} s (*dashed lines*), given $T_k = 100$ K. For HCN column densities, multiply N_{CO} by [HCN]/[CO] $= 2.5 \times 10^{-4}$.

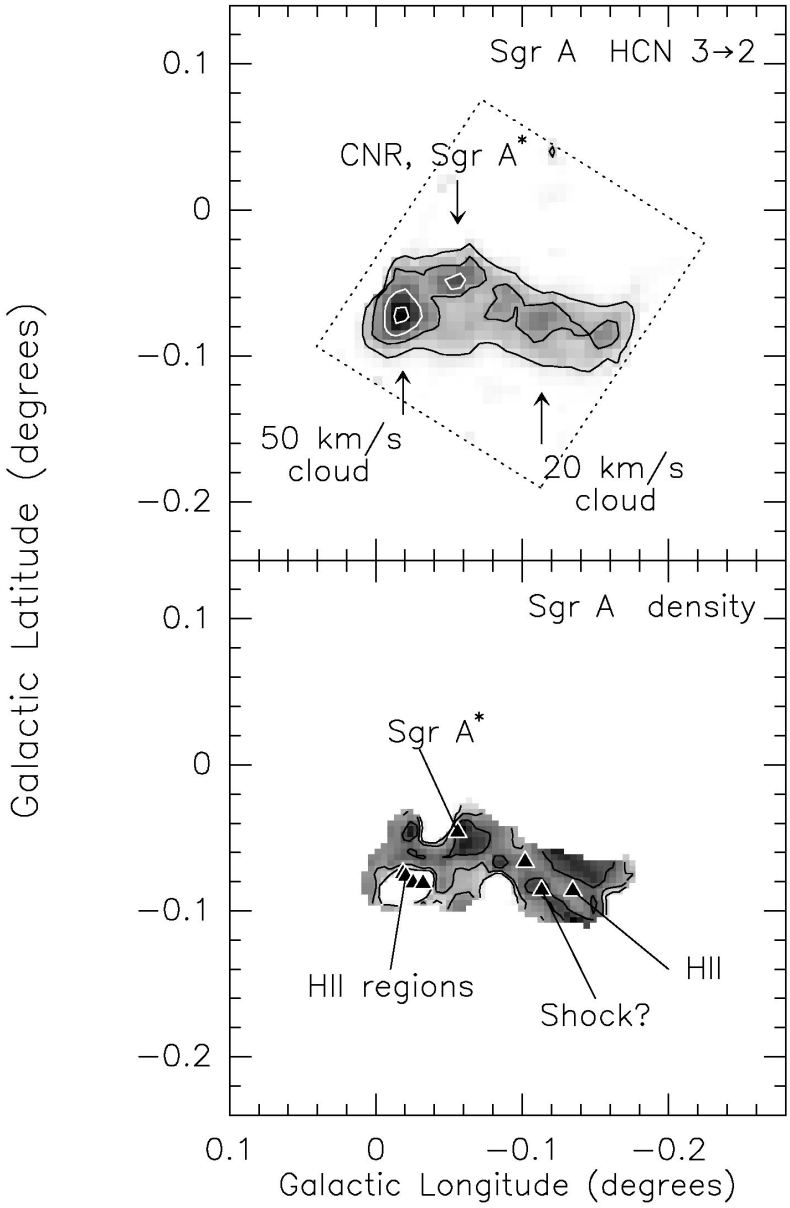

FIG. 11.—*Top*: Map of the integrated HCN $J = 3 \rightarrow 2$ emission from Sgr A. Contours are 200, 300, 400, and 500 K km s^{-1}. Dotted line outlines the mapped region. *Bottom*: Map of density in Sgr A with radio continuum sources (*triangles*) (Ho et al. 1985). Contours are log $(n_{H_2}/cm^{-3}) = 4.0, 4.5$, and 5.0.

B appears warmer and has a narrower range of column densities. The larger dispersion in Δv(HCN) for Sgr A may account for its broader distribution of estimated column densities. In general, the distributions for Sgr A are broader than those of Sgr B. This difference, plus the larger mass fraction of low n_{H_2} and ϕ solutions in Sgr A, support the interpretation that the clouds there may be perturbed (see § 3.3).

TABLE 2

MODEL RESULTS FOR SGR A AND SGR B

Cloud	f_1	[HCN]/[CO]	$\langle T_k \rangle$ (K)	$\langle \log (N_{HCN}/\Delta v) \rangle$ (cm^{-2} km^{-1} s)	$\langle \log n \rangle$ (cm^{-3})	$\langle \phi \rangle$
Sgr A.....	0.1	2.5×10^{-4}	97 ± 26	14.1 ± 0.4	4.5 ± 0.4	0.3 ± 0.2
Sgr B.....	0.1	2.5×10^{-4}	138 ± 24	14.1 ± 0.1	4.5 ± 0.4	0.2 ± 0.1

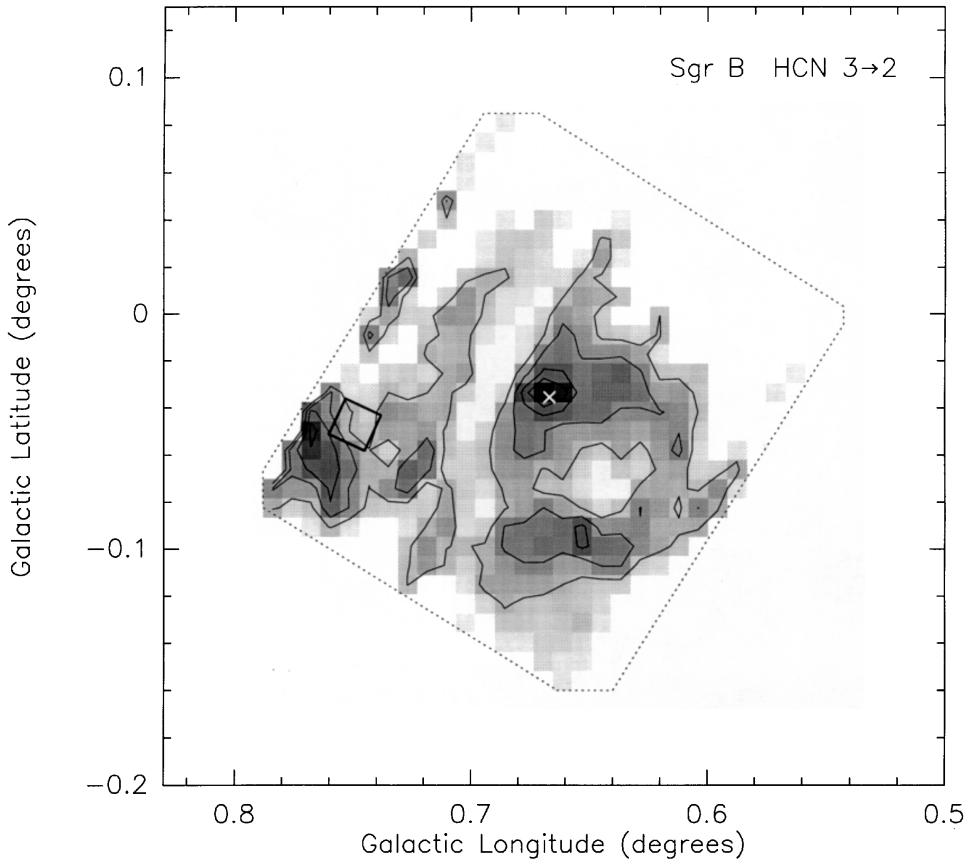

FIG. 12.—Map of the HCN $J = 3 \rightarrow 2$ emission from Sgr B. Contours are 160, 220, 280, and 340 K km s^{-1}. Dotted line outlines the mapped region. The tilted box indicates the location and positional errors of FIR source 38 from the survey of Odenwald & Fazio (1984). The white cross marks the location of Sgr B2 Main (Benson & Johnston 1984).

It is interesting to note that the highest densities derived for the Sgr A clouds are not located at the 50 km s^{-1} cloud, the peak of the HCN $J = 3 \rightarrow 2$ emission, but at the circumnuclear ring around Sgr A* and the 20 km s^{-1} cloud (Fig. 11). In fact, the H II regions in Sgr A may reside in relatively low-density areas because they have cleared out some of the gas. However, the CNR and the shock-compressed region of the 20 km s^{-1} cloud (Ho et al. 1985) are density peaks.

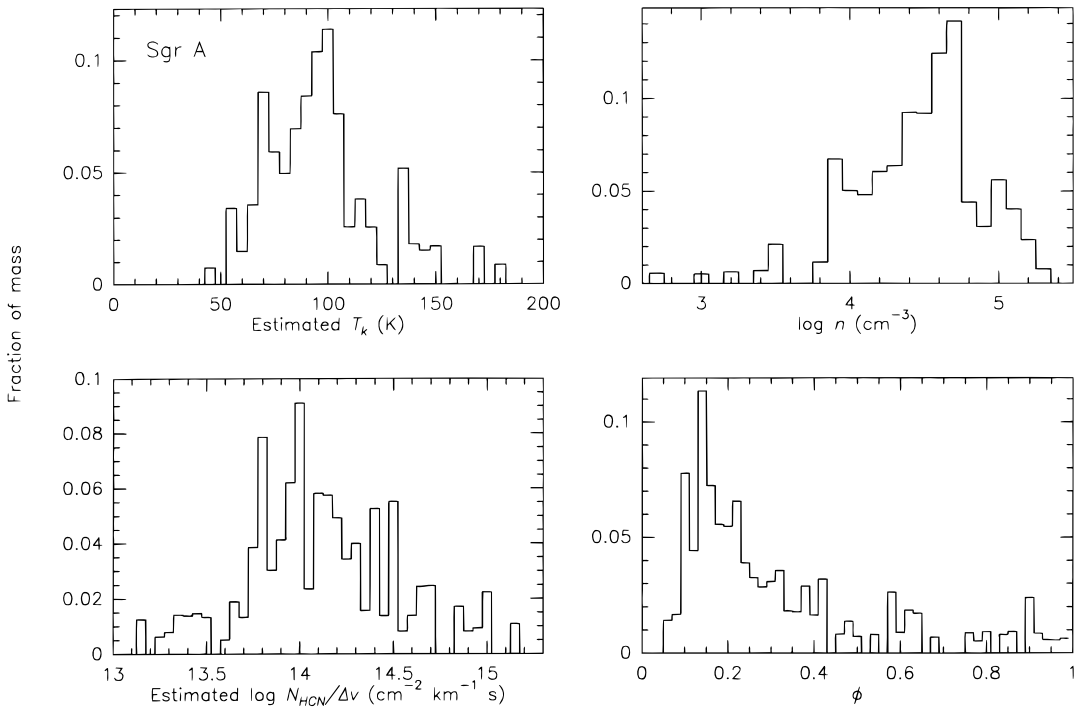

FIG. 13.—Fraction of mass as plotted in Fig. 1 for Sgr A from the analysis of HCN $J = 3 \rightarrow 2/J = 1 \rightarrow 0$. Here $f_1 = 0.1$.

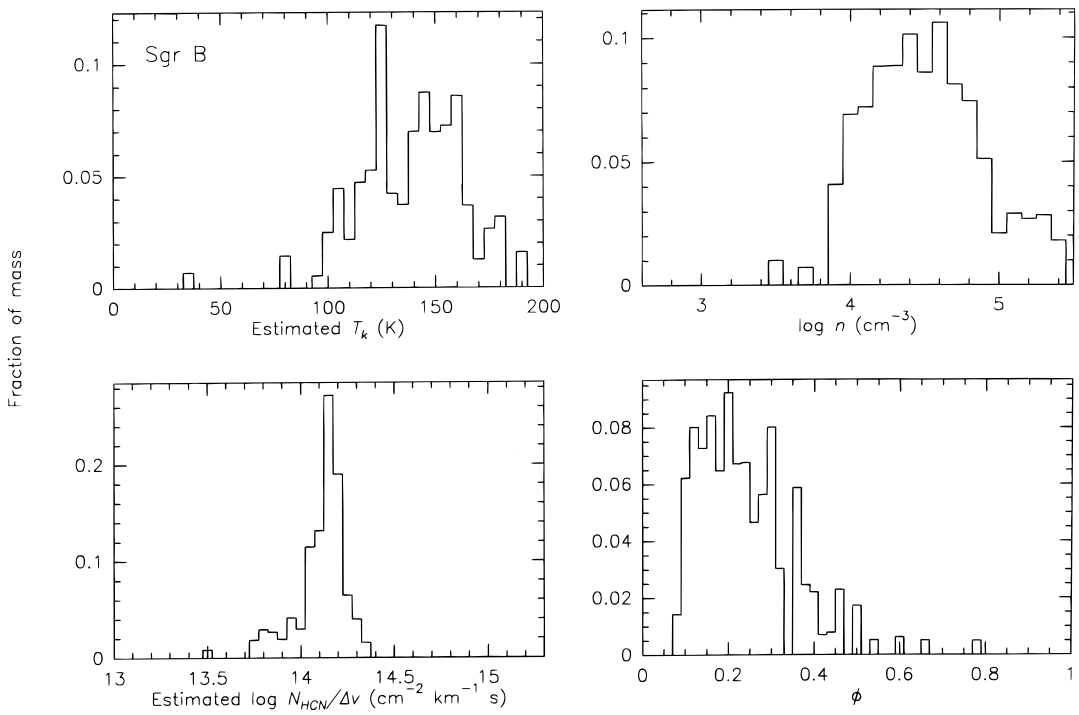

FIG. 14.—Same as Fig. 13, for Sgr B

Therefore, this technique successfully identifies density enhancements not obvious as brightness peaks. That we are able to discern these features despite our limited resolution shows the reliability of HCN $J = 3 \rightarrow 2/J = 1 \rightarrow 0$ as a measure of molecular gas densities in giant molecular clouds.

3.4.4. *Model Biases*

To determine the biases in the model and procedure, 100 HCN $J = 3 \rightarrow 2$, HCN $J = 1 \rightarrow 0$, and CO $J = 1 \rightarrow 0$ intensities were generated from random inputs, as in § 3.1.4. The output parameters are plotted against the inputs in Figure

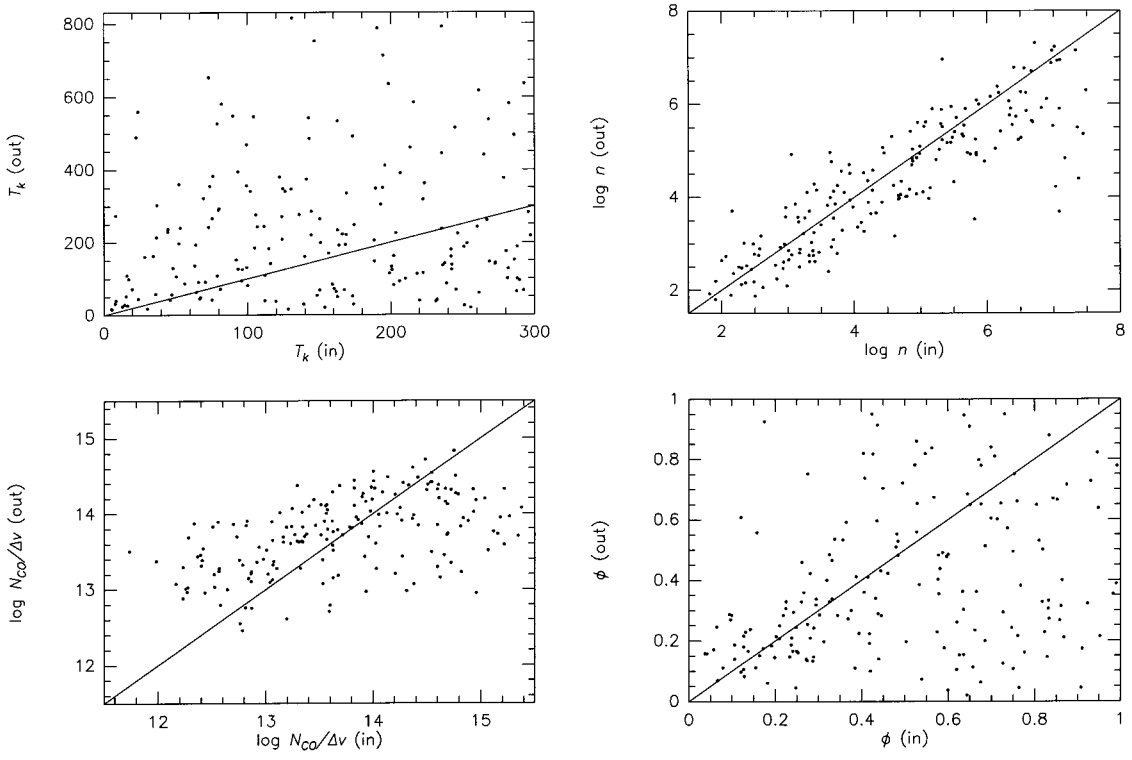

FIG. 15.—Model solutions plotted against random inputs using HCN $J = 3 \rightarrow 2/J = 1 \rightarrow 0$. Here $f_1 = 0.1$. A slope of unity is indicated.

15, for $f_1 = 0.1$ and [HCN]/[CO] $= 2.5 \times 10^{-4}$. The biases from this analysis are similar to those from the HCN/CO ratio, although nearly all input densities are recovered using HCN $J = 3 \rightarrow 2/J = 1 \rightarrow 0$.

3.5. *Comparing HCN $J = 3 \rightarrow 2/J = 1 \rightarrow 0$ with $\mathscr{R}$*

Slightly higher average densities are found from the HCN $J = 3 \rightarrow 2/J = 1 \rightarrow 0$ ratio than from the HCN/CO analysis (Fig. 16). The logarithms of the CO and HCN column densities differ by 3.3 ± 0.3, nearly the chosen abundance ratio of log [HCN]/[CO] $= -3.6$. (The extra factor of 0.3 arises because $\Delta v_{CO} \sim 2 \times \Delta v_{HCN}$). Thus, we find self-consistency in the model despite the known biases.

In Figure 17, the HCN $J = 3 \rightarrow 2/J = 1 \rightarrow 0$ ratio is shown versus $\mathscr{R}$. These ratios were modeled to find a physical basis for the differences in the derived densities. The homogeneous cloud model cannot simultaneously account for the two ratios. For a given value of HCN $J = 3 \rightarrow 2/J = 1 \rightarrow 0$, the model predicts a higher HCN/CO ratio. This results again because $\phi(\mathrm{CO}) > \phi(\mathrm{HCN})$. Therefore, the observed $\mathscr{R}$ is a lower limit to the actual ratio, and the real cloud is not homogeneous. This error is most pronounced

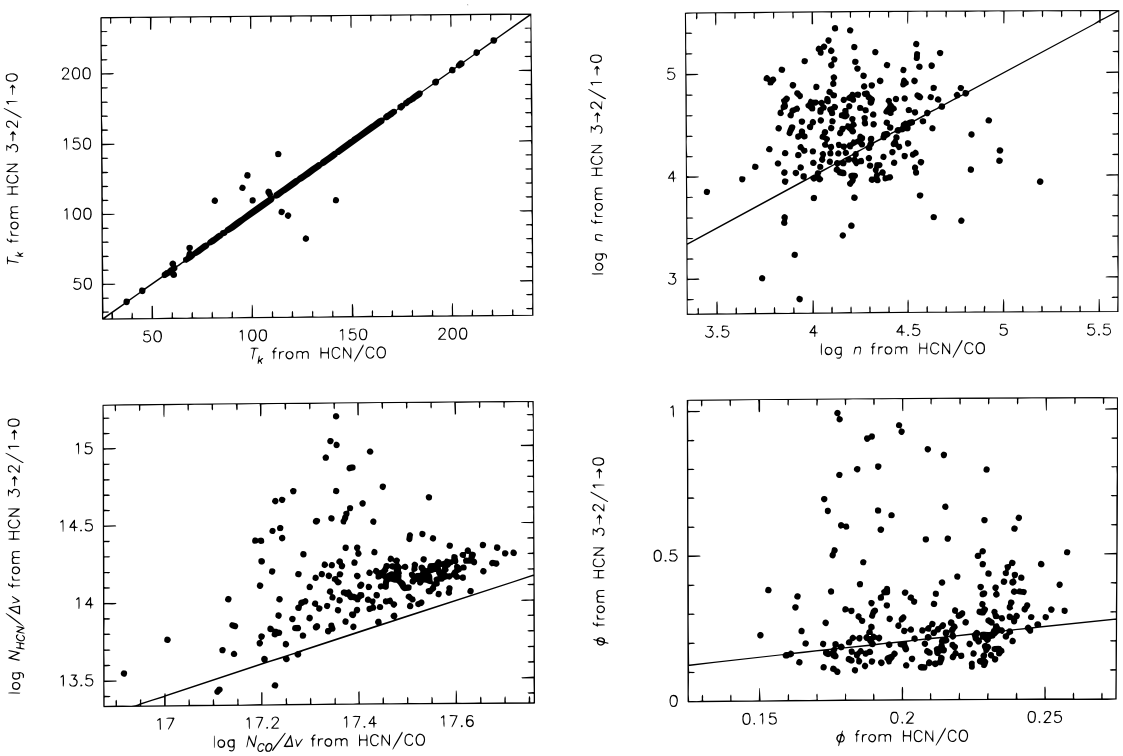

FIG. 16.—Comparison between solutions from analyzing HCN $J = 3 \rightarrow 2/J = 1 \rightarrow 0$ and $\mathscr{R}$. A slope of unity is indicated. For column density, an offset of log [HCN]/[CO] $= -3.6$ was included.

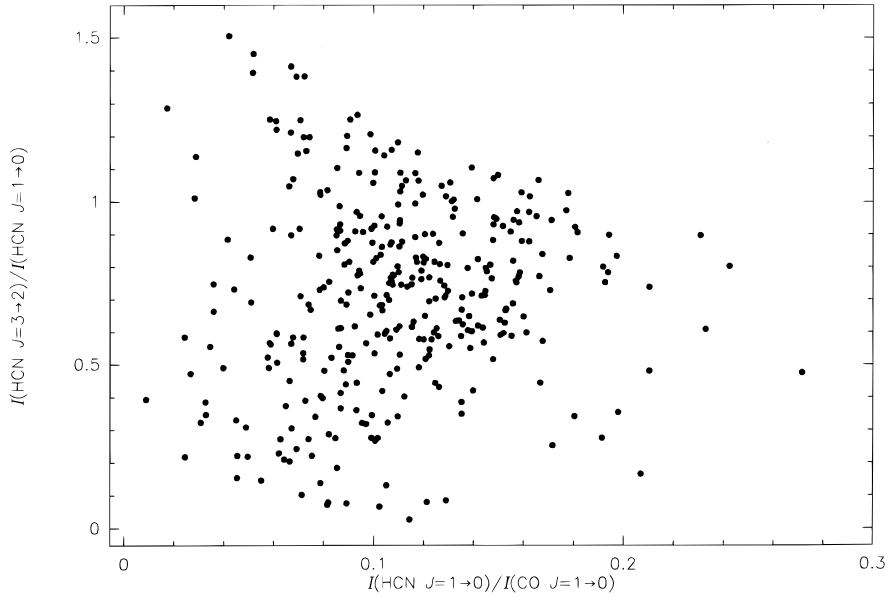

FIG. 17.—Comparison between HCN $J = 3 \rightarrow 2/J = 1 \rightarrow 0$ and $\mathscr{R}$

at the cloud edges, where the HCN emission fades, yet the densities are sufficient to excite the CO line.

4. SUMMARY

We made wide-field maps of the emission from dense molecular gas in the Galactic center. The HCN/CO ratio $\mathscr{R}$ and the HCN $J = 3 \rightarrow 2/J = 1 \rightarrow 0$ ratio were used to estimate the physical properties of the mapped regions.

When convolved to the spatial resolution of extragalactic measurements, the HCN and CO spectra from the Milky Way closely resemble those observed from other galaxies. The density derived from the convolved spectra of the Milky Way was identical to the mean density found by modeling individual map positions. This result implies that similar measurements of other galaxies are most likely sensitive to the *average* properties of their molecular cloud populations, despite poor spatial resolution.

Most of the mass in the Galactic center traced by HCN and CO $J = 1 \rightarrow 0$ is at rather high densities ($n_{H_2} \sim 10^4$ cm^{-3}), roughly an order of magnitude higher than typical values in the disk. The gas features are nearly resolved on parsec scales. The density structure found from modeling the HCN $J = 3 \rightarrow 2/J = 1 \rightarrow 0$ ratio corresponds to known sites of star formation, interaction zones, and the circumnuclear ring around Sgr A*.

Overall, the HCN/CO ratio is a useful probe of the molecular gas properties in the Galactic center and, most likely, other galaxies. It is apparently quite sensitive to pressure, $P = nT_k$, over a wide range of values. However, the derived properties depend on initial assumptions. With only HCN and CO $J = 1 \rightarrow 0$ data, the beam-filling factor is poorly constrained and the resulting column densities and temperatures are biased. As a result, the derived densities depend on ϕ as well, but they are affected most by the chosen [HCN]/[CO] abundance ratio. Also, because the beam-filling factors of HCN and CO are so different, models of homogeneous clouds should be used with caution when analyzing the HCN/CO ratio. On the other hand, the HCN $J = 3 \rightarrow 2/J = 1 \rightarrow 0$ ratio can be modeled without knowing the abundance of HCN, and with less uncertainty in relative beam filling.

This work was funded in part by NSF grant AST 93-18849.

REFERENCES

Aalto, S., Booth, R. S., Black, J. H., & Johansson, L. E. B. 1995, A&A, 300, 369
Benson, J. M., & Johnston, K. J. 1984, ApJ, 277, 181
Bergin, E. A., Langer, W. D., & Goldsmith, P. F. 1995, ApJ, 441, 222
Blake, G. A., Sutton, E. C., Masson, C. R., & Phillips, T. G. 1987, ApJ, 315, 621
Brouillet, N., & Schilke, P. 1993, A&A, 277, 381
Downes, D., Radford, S. J. E., Guilloteau, S., Guélin, M., Greve, A., & Morris, D. 1992, A&A, 262, 424
Erickson, N. R., Goldsmith, P. F., Novak, G., Grosslein, R. M., Viscuso, P. J., Erickson, R. B., & Predmore, C. R. 1992, IEEE Trans. Microwave Theory & Techniques, 40, 1
Flower, D. R., & Launay, J. M. 1985, MNRAS, 214, 271
Frerking, M. A., Langer, W. D., & Wilson, R. W. 1982, ApJ, 262, 590
Gierens, K. M., Stutzki, J., & Winnewisser, G. 1992, A&A, 259, 271
Green, S., & Thaddeus, P. 1974, ApJ, 191, 653
Güsten, R. 1989, in IAU Symp. 136, The Center of the Galaxy, ed. M. Morris (Dordrecht: Kluwer), 89
Güsten, R., & Downes, D. 1980, A&A, 87, 6
Helfer, T. T., & Blitz, L. 1993, ApJ, 419, 86
———. 1997, ApJ, 478, 162
Ho, P. T. P., Jackson, J. M., Barrett, A. H., & Armstrong, J. T. 1985, ApJ, 288, 575
Hüttemeister, S., Wilson, T. L., Bania, T. M., & Martin-Pintado, J. 1993, A&A, 280, 255
Jackson, J. M., Geis, N., Genzel, R., Harris, A. I., Madden, S., Poglitsch, A., Stacey, G. J., & Townes, C. H. 1993a, ApJ, 402, 173
Jackson, J. M., Heyer, M., Paglione, T. A. D., & Bolatto, A. D. 1996, ApJ, 456, L91 (Paper 1)
Jackson, J. M., Paglione, T. A. D., Carlstrom, J. E., & Rieu, N.-Q. 1995, ApJ, 438, 695
Jackson, J. M., Paglione, T. A. D., Ishizuki, S., & Rieu, N.-Q. 1993b, ApJ, 418, L13
Kohno, K., Kawabe, R., Tosaki, T., & Okumura, S. 1996, ApJ, 461, L29
Morris, M. 1993, ApJ, 408, 469
Odenwald, S. F., & Fazio, G. G. 1984, ApJ, 283, 601
Paglione, T. A. D. 1996, Ph.D. thesis, Boston University
Paglione, T. A. D., Jackson, J. M., & Ishizuki, S. 1997a, ApJ, 484, 656
Paglione, T. A. D., Tosaki, T., & Jackson, J. M. 1995, ApJ, 454, L117
Paglione, T. A. D., Yam, O., Heyer, M. H., & Jackson, J. M. 1997b, in preparation
Rieu, N.-Q., Jackson, J. M., Henkel, C., Truong-Bach, & Mauersberger, R. 1992, ApJ, 399, 521
Sakamoto, S. 1996, ApJ, 462, 215
Sanders, R. H., & Lowinger, T. 1972, AJ, 77, 292
Scoville, N. Z., Yun, M. S., Clemens, D. P., Sanders, D. B., & Waller, W. H. 1987, ApJS, 63, 821
Serabyn, E., Lacy, J. H., & Achtermann, J. M. 1992, ApJ, 395, 166
Spergel, D. N., & Blitz, L. 1992, Nature, 357, 665
Sodroski, T. J., et al. 1995, ApJ, 452, 262
Solomon, P. M., Downes, D., & Radford, S. J. E. 1992, ApJ, 387, L55
Stutzki, J., & Winnewisser, G. 1985, A&A, 144, 13